REPORT DOCUMENTATION PAGE

Form Approved
OMB NO. 0704-0188

1. AGENCY USE ONLY (Leave Blank)	2. REPORT DATE 11/17/2006	3. REPORT TYPE AND DATES COVERED Peer-Reviewed Reprint

4. TITLE AND SUBTITLE
"Quasi-wavelet models of turbulent temperature fluctuations" Boundary-Layer Meteorology, V. 120, p. 1-23 (2006).

5. FUNDING NUMBERS
DAAD19-03-1-0104

6. AUTHOR(S)
G.H. Goedecke, D.K. Wilson, and V.E. Ostashev,

7. PERFORMING ORGANIZATION NAME(S) AND ADDRESS(ES)
Physics Department, New Mexico State University,
Box 30001, Dept. 3D, Las Cruces, NM 88003

8. PERFORMING ORGANIZATION REPORT NUMBER

9. SPONSORING / MONITORING AGENCY NAME(S) AND ADDRESS(ES)

U. S. Army Research Office
P.O. Box 12211
Research Triangle Park, NC 27709-2211

10. SPONSORING / MONITORING AGENCY REPORT NUMBER

45258.10-EV-HSI

11. SUPPLEMENTARY NOTES
The views, opinions and/or findings contained in this report are those of the author(s) and should not be construed as an official Department of the Army position, policy or decision, unless so designated by other documentation.

12 a. DISTRIBUTION / AVAILABILITY STATEMENT

Approved for public release; distribution unlimited.

12 b. DISTRIBUTION CODE

13. ABSTRACT (Maximum 200 words)

See the manuscript attached.

14. SUBJECT TERMS

15. NUMBER OF PAGES
23

16. PRICE CODE

17. SECURITY CLASSIFICATION OR REPORT	18. SECURITY CLASSIFICATION ON THIS PAGE	19. SECURITY CLASSIFICATION OF ABSTRACT	20. LIMITATION OF ABSTRACT
UNCLASSIFIED	**UNCLASSIFIED**	**UNCLASSIFIED**	**UL**

Boundary-Layer Meteorology (2006) 120: 1–23
DOI 10.1007/s10546-005-9037-1

QUASI-WAVELET MODELS OF TURBULENT TEMPERATURE FLUCTUATIONS

GEORGE H. GOEDECKE[1,*], D. KEITH WILSON[2]
and VLADIMIR E. OSTASHEV[3]
[1] *Physics Department, New Mexico State University, Las Cruces, NM 88003, U.S.A.;* [2] *U.S. Army Engineer Research and Development Center, 72 Lyme Rd., Hanover, NH 03755, U.S.A.;* [3] *NOAA/Environmental Technology Laboratory, 325 Broadway, Boulder, CO 80305, U.S.A. and Physics Department, New Mexico State University, Las Cruces, NM 88003, U.S.A.*

(Received in final form 11 October 2005 / Published online: 7 July 2006)

Abstract. Here, we contribute to the continuing development of the quasi-wavelet (QW) model of turbulence that is currently being used in simulations of sound propagation and scattering in the turbulent atmosphere. We show that a QW model of temperature fluctuations exists for any physically reasonable temperature spectrum of isotropic homogeneous turbulence, including the widely used von Kármán spectrum. We derive a simple formula for the QW shape that reproduces a given spectrum exactly in the energy, transition, and inertial subranges. We also show that simple QW shapes can be normalized to yield an analytic expression for a temperature spectrum that is fairly close to any given spectrum. As an example, we match the Gaussian QW model to the von Kármán spectrum as closely as possible, and find remarkably good agreement in all subranges including the dissipation subrange. We also derive formulae for the variance and kurtosis associated with the QW model, and show how the latter depends on the QW packing fraction and size distribution. We also illustrate how the visual appearance of several QW-simulated temperature fluctuation fields depends on the QW packing fraction, size distribution, and kurtosis.

Keywords: Quasi-wavelet, Temperature fluctuations, Temperature spectra, Turbulent spectra, von Kármán spectrum.

1. Introduction

Analytical and numerical modelling of turbulent fluctuations is important in several fields, including turbulence theory, boundary-layer meteorology, and wave propagation in turbulent media. During the past several years, we have been developing the quasi-wavelet (QW) models of the velocity and temperature fluctuations of atmospheric turbulence. These models had their

* E-mail: ggoedeck@nmsu.edu

origins in work by McBride et al. (1992), deWolf (1993), Boulanger et al. (1995), and Goedecke and Auvermann (1997). In such models, turbulence is represented as a collection of self-similar localized structures of many different sizes. Originally, these structures were called turbules (McBride et al., 1992; Goedecke and Auvermann, 1997) or eddies (Goedecke et al., 2001a). Now we call them quasi-wavelets (QWs), because they are similar to wavelets. However, QW sizes, shapes, amplitudes, number densities, positions and orientations may be chosen as desired, which is not the case for wavelets. Also, QWs do not satisfy the fluid equations or any orthonormality conditions. Goedecke and Auvermann (1997) showed that the Kolmogorov inertial subrange spectral densities of the velocity and temperature fluctuations of isotropic homogeneous turbulence are reproduced by the QW model if the number densities and amplitudes of the QWs are scaled properly with size, and the sizes are chosen appropriately. They also showed that the QW model automatically predicts the existence of energy and dissipation subranges, and reasonable behaviour of the spectral densities in those subranges.

An important application of the QW model is in simulations of the temperature and velocity fluctuations needed to describe electromagnetic and sound wave propagation and scattering in a turbulent medium. There are already several examples of the successful use of QWs in atmospheric acoustics. First, QWs were used in numerical simulations to predict the detailed properties of Doppler broadened temporal spectra of monochromatic sound waves scattered by atmospheric turbulence advecting with the mean wind (Goedecke et al., 2001a). The results allowed us to explain the properties of experimentally determined Doppler broadened spectra. Second, QWs were employed to study sound scattering due to atmospheric turbulence behind noise barriers (Wilson et al., 2004a), which is an important problem in noise control. Third, QWs were used to model atmospheric turbulence in finite-difference time-domain simulations of sound propagation outdoors (Marlin et al., 2003; Van Renterghem, 2003; Wilson et al., 2003), which is a very promising method in computational atmospheric acoustics. Fourth, QWs were employed in the solution of a forward problem in acoustic tomography of the atmosphere (Vecherin et al., 2004; Wilson et al., 2004b). In the first three of these applications, a kinematic simulation using random Fourier modes (as described, for example, by Fung et al., 1992) would have been impossible or difficult; in the fourth application, QWs were more convenient to use than random Fourier modes.

An important feature of the QW model is that it can provide a virtually exact representation of any physically reasonable spectral density of isotropic homogeneous velocity fluctuations (Goedecke et al., 2004b). In that paper, a simple formula for the unique QW shape associated with a given

velocity spectrum was derived, and, as an example, the unique QW shape that produces the widely-used von Kármán velocity spectrum from the QW model equations was obtained.

Another important feature of the QW model is its ability to represent anisotropic, inhomogeneous, and/or intermittent turbulence. Random Fourier mode representations cannot do this, and orthonormal wavelet representations are more difficult to use than QW representations. We will discuss briefly in Section 3 how to modify current QW models in order to represent inhomogeneity and intermittency. Here, we note that a QW representation of anisotropic velocity fluctuations is under development (Goedecke et al., 2001b, 2004a). The current version of the model is able to match experimental data presented by Mann (1994) quite well, except at very small wavenumbers.

The QW model could be used to simulate virtually any scalar random field, e.g., fluctuations of concentrations of chemical species or the optical refractive index in the atmosphere. In this paper, which complements that of Goedecke et al. (2004b), we focus on QW models of atmospheric temperature fluctuations. The main goals are (i) to investigate how accurately a QW model can reproduce a given spectrum of isotropic homogeneous temperature fluctuations, such as the widely used von Kármán spectrum; (ii) to determine how well a given spectrum can be matched by a QW model with simple QW shapes that are easy to use in numerical simulations and that also provide an analytic form for the spectrum; (iii) to determine how another important property of the modelled turbulent fields, the kurtosis (normalized fourth moment), depends on the QW packing fraction and size distribution; and iv) to illustrate how the visual appearance of several QW simulations depends on the QW packing fraction, size distribution, and kurtosis.

In what follows, in Section 2 we derive a simple QW model of isotropic homogenous temperature fluctuations, and show how well these goals have been achieved. In Section 3, we discuss our results.

2. QW Model of Turbulent Temperature Spectra

2.1. Isotropic QW model

In this subsection and the next, we present a derivation of what is probably the simplest possible QW model of the spectral density of the temperature fluctuations of isotropic homogeneous atmospheric turbulence. In this model, the QWs are all located inside a volume V chosen large enough to contain many QWs of each size. For isotropic temperature spectra, the temperature fluctuation $\Delta T^{\alpha n}(\mathbf{r})$ for each QW is chosen to have the form

$$\Delta T^{\alpha n}(\mathbf{r}) = h^{\alpha n} \Delta T_\alpha f\left(\left|\mathbf{r} - \mathbf{b}^{\alpha n}\right| / a_\alpha\right). \tag{1}$$

Here, $\mathbf{r}$ is the position vector; f is the spatial parent function, spherically symmetric about its centre point, the same for all QWs; α is the size class index, $\alpha = 1, \ldots, N$, where N is the number of size classes; a_α is the QW size in class α, with a_1 the largest, a_N the smallest; "αn" means "nth QW in size class α", $n = 1, \ldots, N_\alpha$, so that N_α is the number of QWs in size class α, and $N_V = \sum_{\alpha=1}^{N} N_\alpha$ is the total number of QWs in V; $\mathbf{b}^{\alpha n}$ is the location of the centre of the (αn)th QW; $\Delta T_\alpha > 0$ is the temperature fluctuation amplitude of all QWs in size class α; and $h^{\alpha n}$ is a random sign factor, ± 1 with equal probability. Also, the $h^{\alpha n}$ are assumed to be statistically independent. Therefore

$$\left\langle h^{\alpha n} \right\rangle = 0, \tag{2a}$$

$$\left\langle h^{\alpha n} h^{\beta m} \right\rangle = \delta_{\alpha\beta} \delta_{nm}, \tag{2b}$$

where, δ_{nm} and $\delta_{\alpha\beta}$ are Kronecker symbols. The total temperature fluctuation $\Delta T(\mathbf{r})$ in V is the sum

$$\Delta T(\mathbf{r}) = \sum_{\alpha=1}^{N} \sum_{n=1}^{N_\alpha} \Delta T^{\alpha n}(\mathbf{r}). \tag{3}$$

In this model, the locations $\{\mathbf{b}^{\alpha n}\}$ are uniformly random and statistically independent in V, which ensures that the fluctuations are homogeneous in V, except within a distance of order a_1 from the edges of V. The quantities ΔT_α, N, and N_α are not stochastic variables.

Figure 1 depicts a sample simulation of two-dimensional isotropic homogeneous turbulent temperature fluctuations by circularly symmetric QWs of different sizes. A solid circle corresponds to a positive QW amplitude, with $h^{\alpha n} = +1$; a dashed circle corresponds to a negative QW amplitude, with $h^{\alpha n} = -1$. The point O is the arbitrarily located origin. Several position vectors $b^{\alpha n}$ and sizes a_α are indicated. Only four size classes are used in this sample ($N = 4$), and, in each size class, the number of QWs with positive amplitudes equals the number with negative amplitudes. (This is not a necessary condition; only the statistical mean temperature fluctuation over an ensemble of such samples must vanish). For simplicity, in this sample the ratio of $N_{\alpha+1}$ to N_α was chosen to be two, with $N_1 = 2$. In a realistic simulation, both N_1 and N would be larger, and the ratio $N_{\alpha+1}/N_\alpha$ would be smaller.

In what follows, we need the Fourier transform $\Delta\tilde{T}(\mathbf{k})$ of the temperature fluctuation, written as a superposition of the Fourier transforms $\Delta\tilde{T}^{\alpha n}(\mathbf{k})$ of the individual QW fluctuations. These expressions are given by

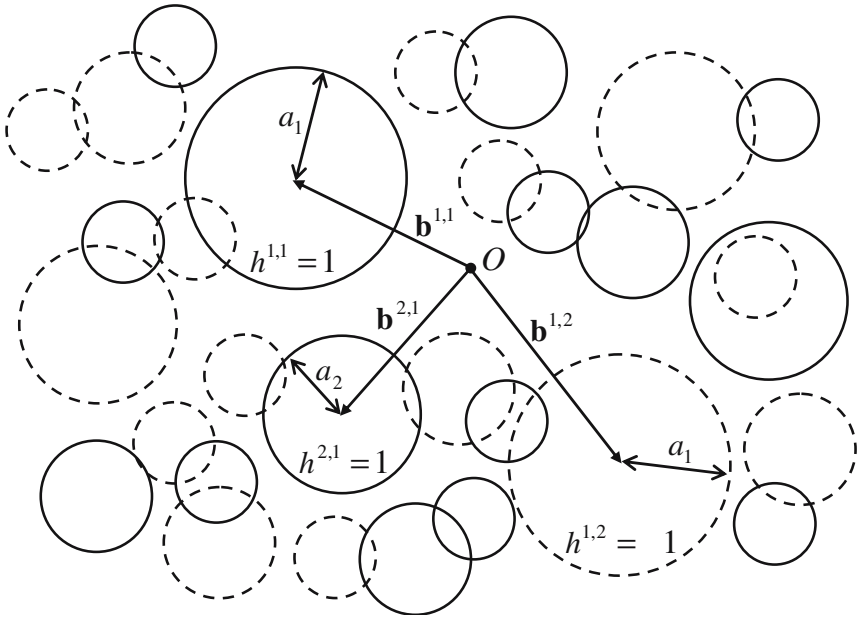

Figure 1. QW simulation of a two-dimensional turbulent temperature fluctuation.

$$\Delta\tilde{T}(\mathbf{k}) \equiv (2\pi)^{-3} \int d^3r \Delta T(r) \exp(-i\mathbf{k}\cdot\mathbf{r}) = \sum_{\alpha=1}^{N} \sum_{n=1}^{N_\alpha} \Delta\tilde{T}^{\alpha n}(\mathbf{k}), \tag{4a}$$

$$\Delta\tilde{T}^{\alpha n}(\mathbf{k}) = h^{\alpha n} a_\alpha^3 \Delta T_\alpha \exp\left(-i\mathbf{k}\cdot\mathbf{b}^{\alpha n}\right) F(ka_\alpha), \tag{4b}$$

$$F(y) \equiv (2\pi)^{-3} \int d^3\xi \exp(-i\boldsymbol{y}\cdot\boldsymbol{\xi}) f(\xi). \tag{4c}$$

Here and below, $k \equiv |\mathbf{k}|$, $y \equiv |\mathbf{y}|$, etc. The dimensionless Fourier transform $F(y)$ is called the spectral parent function. In general, in this simplest model we do not allow $F(0) = 0$, whereby, according to Equation (4c), f must have a non-zero spatial integral. Therefore, we may choose the normalization $F(0) = 1$ with no loss of generality, and for convenience we do so.

2.2. QW TEMPERATURE SPECTRUM

Under the conditions discussed in Section 2.1, the general expression for the temperature fluctuation spectrum $\Phi^T(\mathbf{k})$ is easily shown to be

$$\Phi^T(\mathbf{k}) = \frac{(2\pi)^3}{V} \left\langle \left| \Delta\tilde{T}(\mathbf{k}) \right|^2 \right\rangle = (2\pi)^{-3} \int d^3r e^{-i\mathbf{k}\cdot\mathbf{r}} B^T(\mathbf{r}), \tag{5}$$

where $B^T(\mathbf{r})$ is the autocorrelation function $\langle \Delta T(\mathbf{r}_1 + \mathbf{r}) \Delta T(\mathbf{r}_1) \rangle$. Inserting the QW expressions (4a) and (4b) for $\Delta \tilde{T}(k)$ in terms of the $\Delta \tilde{T}^{\alpha n}(\mathbf{k})$ yields

$$\Phi^T(\mathbf{k}) = (2\pi)^3 \sum_{\alpha=1}^{N} n_\alpha a_\alpha^6 (\Delta T_\alpha)^2 F^2(\mathbf{k} a_\alpha), \tag{6}$$

with $n_\alpha = N_\alpha / V$, so that n_α is the mean number density of QWs of size a_α in V. Note that any spherically symmetric spatial parent function (as in Equation (1)) yields a spherically symmetric spectral parent function (as in Equation (4c)), which in turn yields an isotropic temperature spectrum, i.e., a spectrum that depends only on the magnitude k of the wavevector $\mathbf{k}$.

In order to proceed further, we need scaling laws for $\Delta T_\alpha, n_\alpha$, and a_α. We use the following:

$$\Delta T_\alpha = (\Delta T_1)(a_\alpha / a_1)^{1/3}, \tag{7a}$$

$$n_\alpha a_\alpha^3 = \phi, \tag{7b}$$

$$a_\alpha = a_1 e^{-\mu(\alpha - 1)}, \tag{7c}$$

for $\mu > 0$. Here, ϕ and μ are scale-invariant parameters; ϕ is called the packing fraction. Together, these relationships lead to the correct (Kolmogorov) spectral behaviour in the inertial subrange, but they are not the only ones that do so. As discussed in Goedecke and Auvermann (1997), the particular relationships in Equation (7) were chosen because the first agrees with the Kolmogorov energy transfer model of fully developed turbulence; the second enforces a constant packing fraction; and the third yields a fractal sequence of QW sizes, as suggested by Nelkin (1992). Note that the second and third relationships are analogous to those that occur in conventional wavelet analysis. We note again that this same QW model could be used to simulate other scalar random fields that satisfy the scaling relations of Equation (7), or similar ones.

Referring again to the sample two-dimensional simulation depicted in Figure 1, note that, since $N_{\alpha+1} = 2N_\alpha$, the two-dimensional analogue of the second relationship in Equation (7) requires $a_{\alpha+1} = a_\alpha / \sqrt{2}$, which is what was used in the sample simulation. In turn, the third relation in Equation (7) yields $\mu = 0.5 \ln 2$ for this two-dimensional example. Also note that there is considerable overlapping of different QWs in Figure 1, which is expected in general for the uncorrelated random locations used.

In principle, the parameter μ may be chosen small enough that the sum over sizes in Equation (6) may be replaced by an integral, as follows:

$$\sum_{\alpha=1}^{N} (\cdots) \to \int_1^N d\alpha \, (\cdots) = \frac{1}{\mu} \int_{a_N}^{a_1} \frac{da}{a} (\cdots), \tag{8}$$

where the last equality follows from Equation (7c). Using these relations in Equation (6), we obtain

$$\Phi^T(k) = C_1 (k a_1)^{-11/3} \int_{k a_N}^{k a_1} dy\, y^{8/3} F^2(y), \tag{9}$$

where $C_1 \equiv (2\pi)^3 (\phi/\mu) (\Delta T_1)^2 a_1^3$. If the integral is constant over some range of k, then $\Phi^T(k) \propto k^{-11/3}$ in that range, which is thus the inertial subrange. This occurs if $a_N \ll a_1$, for any localized spectral parent function. For example, consider a Gaussian spectral parent function

$$F(y) = \exp(-y^2/2). \tag{10}$$

Inserting this in Equation (9) yields

$$\Phi^T_{\mathrm{G}}(k) = \frac{1}{2} C_1 (k a_1)^{-11/3} \left[\gamma\left(11/6, k^2 a_1^2\right) - \gamma\left(11/6, k^2 a_N^2\right) \right], \tag{11}$$

where $\gamma(p, x) = \int_0^x dt\, t^{p-1} e^{-t}$ is the incomplete gamma function. Its properties imply that this Gaussian QW spectrum is equal to a constant for $k a_1 \ll 1$, behaves like $k^{-11/3}$ for $k a_1 \gg 1 \gg k a_N$, and falls off faster than $k^{-11/3}$ for $k a_N \gtrsim 1$. This general behaviour occurs for all localized parent functions $f(\xi)$ and thus for all isotropic temperature spectra in this simple QW model. The Gaussian spectral parent function is one of two that we have found that yields a simple spatial parent function and also yields a fairly simple analytic expression for the temperature spectrum; the other is an exponential spectral parent function.

2.3. Match to given spectrum

In this subsection, we show that specific spectral and spatial parent functions corresponding to any given physically reasonable isotropic spectrum can be found, and we obtain expressions for the parent functions that correspond to the von Kármán spectrum.

In general, we suppose that $\Phi^T(x)$ is a given analytic function, and we take the derivative $\partial/\partial x$ of the product of $x^{11/3}$ and Equation (9), where $x = k a_1$. This yields

$$\frac{\partial}{\partial \mathrm{x}} \left(x^{11/3} \Phi^T(x) \right) = C_1 x^{8/3} \left(F^2(x) - (a_N/a_1)^{11/3} F^2(a_N x/a_1) \right). \tag{12}$$

In many cases, we are not interested in the dissipation subrange $k a_N > 1$, or the spectrum is not known in that region, or both. In such cases, it is reasonable to neglect the last term above, since typically $a_N/a_1 \lesssim 10^{-3}$. Then Equation (12) yields

$$F^2(x) = C_1^{-1} x^{-8/3} \frac{d}{dx} \left[x^{11/3} \Phi^T(x) \right]. \tag{13}$$

Using this spectral parent function in Equation (9) will reproduce the given spectrum $\Phi^T(ka_1)$ accurately in the energy, transition, and inertial subranges, i.e. for $ka_N < 1$. The corresponding QW spatial parent function will be localized and bounded if $\Phi^T(ka_1)$ falls off fast enough for large k. For example, the widely-used von Kármán spectrum is given by

$$\Phi^T_{\mathrm{VK}}(k) = C_{\mathrm{VK}} \left(1 + L_s^2 k^2\right)^{-11/6} \exp(-k^2 l^2), \tag{14}$$

where (L_s, l) are (outer, inner) scale lengths, and C_{VK} is the value of the spectrum at $k = 0$. If we use this in Equation (13), we obtain a QW spectral parent function

$$F_{\mathrm{VK}}(x) \approx \left(1 + L_s^2 x^2 / a_1^2\right)^{-17/12} \exp(-x^2 l^2 / 2a_1^2). \tag{15}$$

In obtaining this result, we put $C_1 = (11/3) C_{\mathrm{VK}}$ in order to normalize $F_{\mathrm{VK}}(0)$ to unity. For simplicity, we also dropped a term resulting from the derivative of the Gaussian function in Equation (14), because that term is negligibly small for $kl \ll 1$, which is the region of interest. If we substitute Equation (15) into Equation (9), the resulting QW spectrum is equal to the von Kármán spectrum to extremely high accuracy for all $k \ll 1/l$. In principle this is true for almost any choice of the ratio L_s/a_1. However, we expect $a_1 \approx L_s$, and we also expect $a_N \approx l$. In what follows, we choose $(l/L_s) = (a_N/a_1)$. The corresponding QW spatial parent function is given by inserting Equation (15) into the inverse of Equation (4c) and integrating over the 4π solid angle in y-space:

$$f_{\mathrm{VK}}(\xi) = 4\pi \xi^{-1} \int_0^\infty dy\, y\, \sin(\xi y)(1 + (L_s y/a_1)^2)^{-17/12} \exp(-y^2 l^2 / 2a_1^2). \tag{16}$$

This is a localized function that is bounded for all ξ if and only if a high-k cut-off such as the Gaussian is present in the von Kármán spectrum. Without the cut-off, the function is unbounded at $\xi = 0$.

2.4. Comparison of Gaussian QW and von Kármán spectra

In this subsection, we show that it is possible to use a simple parent function, such as a Gaussian function, and still achieve a good match to a given spectrum in most spectral regions. To illustrate this, we regard the von Kármán spectrum of Equation (14) as a given spectrum. Then we adjust the parameters of the QW Gaussian spectrum of Equation (11) to match as many of the properties of the given spectrum as possible.

One important property of turbulent temperature fluctuations is their variance, defined by

$$\sigma^2 \equiv B^T(0) = \int d^3k \Phi^T(k), \tag{17}$$

where the second equality follows from the inverse of Equation (5). For the simplified von Kármán spectrum, defined by Equation (14) without the Gaussian cut-off, the variance σ^2_{VK} is related to the amplitude C_{VK} by

$$\sigma^2_{\mathrm{VK}} = \left(\pi^{3/2}\Gamma(1/3)/\Gamma(11/6)\right)\left(C_{\mathrm{VK}}/L_{\mathrm{s}}^3\right). \tag{18}$$

In obtaining this result, we used Equations (8.380.3) and (8.384.2) in Gradshteyn and Rhyzik (1980). It is straightforward to show that the Gaussian cut-off in Equation (14) reduces this result by 2% or less for $a_N/a_1 \lesssim 0.002$, which is satisfied for well-developed, high Reynolds number turbulence. Therefore, Equation (18) provides a good approximation, and we use it in what follows.

In order to obtain a similar relation for the Gaussian QW spectrum, we substitute Equation (11) into Equation (17). This yields

$$\sigma^2_{\mathrm{G}} = \left(2\pi C_1/a_1^3\right)\int_0^\infty dy\, y^{-5/3}\left[\gamma(11/6, y^2) - \gamma(11/6, m^2y^2)\right], \tag{19}$$

where $m = a_N/a_1$, and $y = ka_1$. For $m \lesssim 0.002$, the ratio of the second term on the right-hand side to the first is clearly $m^{2/3} \lesssim 0.016$. The second term is analogous to that resulting from the cut-off in the von Kármán spectrum; for simplicity, we drop the second term. An integration by parts of the first term yields

$$\sigma^2_{\mathrm{G}} \approx \frac{3}{2}\pi^{3/2}C_1/a_1^3. \tag{20}$$

Other important properties of temperature spectra are their behaviours in the inertial and energy subranges. For the von Kármán spectrum of Equation (14), the inertial subrange clearly occurs for $l^{-1} \gg k \gg L_{\mathrm{s}}^{-1}$; for the Gaussian QW spectrum of Equation (11), it occurs for $a_N^{-1} \gg k \gg a_1^{-1}$. In these subranges, Equations (14) and (11) reduce immediately to

$$\Phi^T_{\mathrm{VK}}(k) \approx C_{\mathrm{VK}} L_{\mathrm{s}}^{-11/3} k^{-11/3}, \tag{21a}$$

$$\Phi^T_{\mathrm{G}}(k) \approx \tfrac{1}{2} C_1 \Gamma(11/6) a_1^{-11/3} k^{-11/3}, \tag{21b}$$

which both display the characteristic $k^{-11/3}$ dependence of the inertial subrange. Since we are regarding the von Kármán spectrum as a given spectrum, clearly we must set the two spectra equal in the overlapping part of their inertial subranges. Then Equation (21) yields

$$\frac{C_1}{C_{\mathrm{VK}}} = \frac{2}{\Gamma(11/6)}\left(\frac{a_1}{L_{\mathrm{s}}}\right)^{11/3}. \tag{22}$$

For the von Kármán spectrum, the energy subrange occurs for $k \ll 1/L_s$; for the Gaussian QW spectrum (and all QW spectra) it occurs for $k \ll 1/a_1$. In these subranges, Equations (14) and (11) yield

$$\Phi_{VK}^{T}(k) = C_{VK}, \tag{23a}$$

$$\Phi_{G}^{T}(k) = (3/11)\, C_1. \tag{23b}$$

These are both constants for small k, which is the conventional behaviour of temperature spectra in the energy subrange.

If we apply Equation (22), as we must, and also attempt to put $\sigma_{\mathrm{G}}^2 = \sigma_{\mathrm{VK}}^2$ (Equations (18) and (20)) as well as $\Phi_{\mathrm{G}}^{T}(k) = \Phi_{\mathrm{VK}}^{T}(k)$ for small k (Equations (23)), we clearly overspecify the two unknown parameters C_1/C_{VK} and a_1/L_{s}. For example, we may require the spectra to be equal in the energy subrange, or we may require the fluctuations to have the same variance; but we may not require both. Below, we investigate these alternatives.

2.4.1. *Case i. Spectra Equal in Both Inertial and Energy Subranges*
For this case, we use Equations (22) and (23) to determine the Gaussian QW parameters. This yields

$$a_1/L_{\mathrm{s}} = (\Gamma(17/6))^{3/11} = 1.16, \tag{24a}$$

and

$$C_1/C_{\mathrm{VK}} = 11/3. \tag{24b}$$

Then, Equations (18) and (20) yield the variance ratio

$$\sigma_{\mathrm{G}}^2/\sigma_{\mathrm{VK}}^2 = 1.24. \tag{25}$$

Figure 2 contains log-log plots of the von Kármán and simplified von Kármán spectra, and the Gaussian QW spectrum adjusted to agree with the von Kármán spectra in the inertial and energy subranges, versus wavenumber k. In this example, we made the following choices, which are reasonable for near-ground atmospheric turbulence, $L_{\mathrm{s}} = 10\,\mathrm{m}$; $l = .02\,\mathrm{m}$ with

$$a_N/l = a_1/L_{\mathrm{s}} = 1.16. \tag{26}$$

(see Equation (24)). The plots reveal that this Gaussian QW spectrum is virtually identical to the von Kármán spectrum in the dissipation subrange as well. However, the spectra disagree noticeably in the transition region between the energy and inertial subranges. Apparently, this disagreement is enough to make the variance of the Gaussian QW model fluctuation 24% larger than that of the von Kármán fluctuation (see Equation (25)).

Figure 3 contains plots of the corresponding Gaussian and von Kármán dimensionless spatial parent functions vs. $\xi = r/a_1$, where here r is the

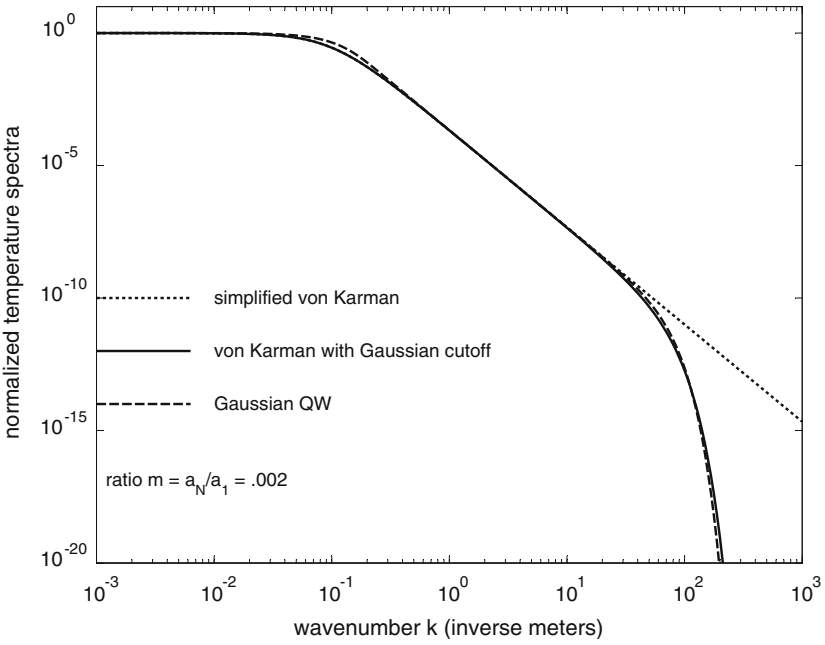

Figure 2. Comparison of Gaussian QW and von Kármán temperature spectra chosen to be equal in the inertial and the energy subranges.

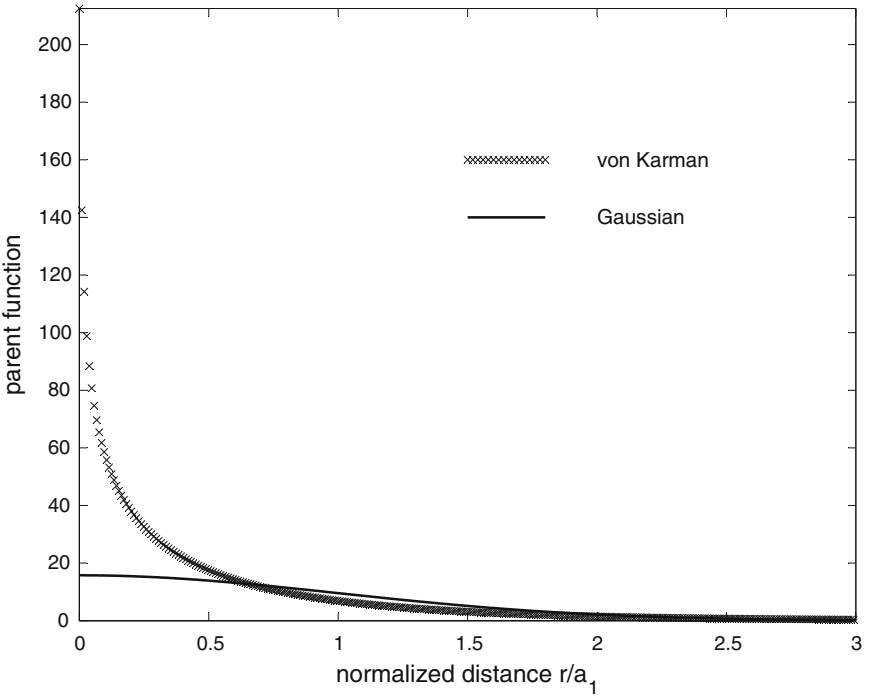

Figure 3. Gaussian and von Kármán spatial parent functions for the conditions in Figure 2.

distance from the centre of the parent function. Using the Gaussian spectral parent function of Equation (10), the corresponding spatial parent function is of course also a Gaussian function, given by

$$f_{\mathrm{G}}(\xi) \equiv \int d^3y F_{\mathrm{G}}(y) \exp(i\mathbf{y}\cdot\boldsymbol{\xi}) = (2\pi)^{3/2} \exp(-\xi^2/2). \tag{27}$$

The von Kármán spatial parent function plotted in Figure 3 was obtained numerically from a fast Fourier transform algorithm applied to Equation (16), using the values given in Equation (26). Although the two spatial parent functions are close for $\xi \gtrsim 0.5$, they differ markedly for small ξ. The von Kármán function increases rapidly as $\xi \to 0$, but it is bounded at $\xi = 0$.

2.4.2. *Case ii. Spectra Equal in Inertial Subrange, with Fluctuations having the Same Variance*

For this case, we use Equations (18), (20), and (22) to determine the Gaussian QW parameters. This yields

$$a_1/L_{\mathrm{s}} = (\Gamma(4/3))^{3/2} = 0.844, \tag{28a}$$

and,

$$C_1/C_{\mathrm{VK}} = 0.724. \tag{28b}$$

Then, Equation (23) yields the small-k (energy subrange) limit

$$\left(\frac{\Phi^T_{\mathrm{G}}(k)}{\Phi^T_{\mathrm{VK}}(k)}\right)_{k\to 0} = \frac{3C_1}{11C_{\mathrm{VK}}} = 0.198. \tag{29}$$

Figure 4 contains log-log plots of the von Kármán and simplified von Kármán spectra, and the Gaussian QW spectrum adjusted to satisfy the conditions of case (ii), versus wavenumber k. In this example, we made the same reasonable choices of parameter values listed in Equation (26), as well as the choices in Equation (28). Clearly, these case (ii) conditions make the spectra differ noticeably everywhere except in the overlapping part of their inertial subranges.

Figure 5 contains plots of the corresponding Gaussian and von Kármán dimensionless spatial parent functions vs. $\xi = r/a_1$, for the conditions of case (ii). The Gaussian spectral parent function of Equation (10) still yields the spatial parent function of Equation (27). However, when plotted vs. ξ, the von Kármán spatial parent function appears to be different in this case than in case (i), because the values of a_1/L_{s} and thus a_N/l are different from those in case (i). Note that the von Kármán spatial parent function is bounded at $\xi = 0$ in this case as well.

Note that our choice $a_1/L_{\mathrm{s}} = a_N/l$ (see Equation (26)) is reasonable but not required. Different choices will affect QW spectra in the dissipation

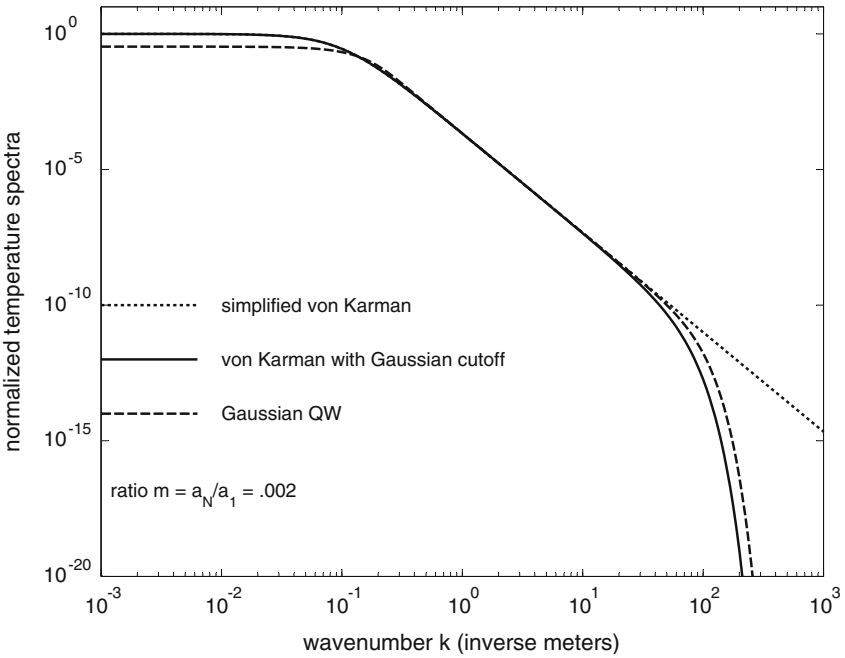

Figure 4. Comparison of QW Gaussian and von Kármán temperature spectra chosen to be equal in the inertial subrange, with fluctuations chosen to have the same variance.

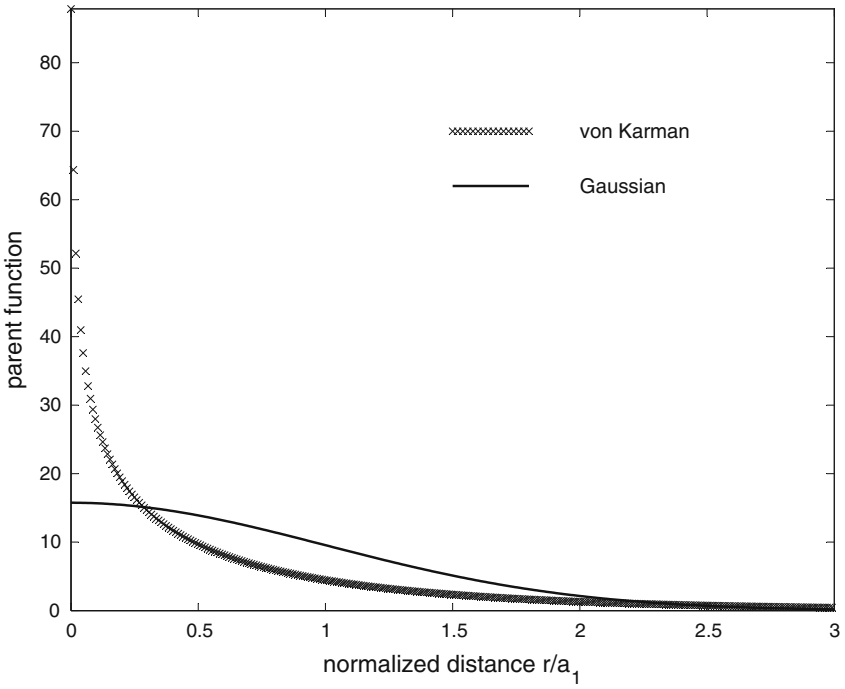

Figure 5. Gaussian and von Kármán spatial parent functions for the conditions in Figure 4.

subrange. For example, we could choose a_N/l to yield good agreement between the Gaussian QW and the von Kármán spectra in this subrange in Figure 4, but that would alter the good agreement between the two in this subrange in Figure 2. In this sense, then, the latter good agreement is merely an artefact of a fortuitous choice.

2.5. Kurtosis in the QW model

In this section, we calculate the kurtosis (normalized fourth moment) of a QW field. As an initial step, the variance (second moment) is calculated by a different method than was used earlier in the text, where the spectrum was integrated to determine the variance. We will require this alternative, more direct method to calculate the kurtosis. Substituting Equation (1) into Equation (3), squaring, and taking the ensemble mean, we have

$$\left\langle \Delta T^2(\mathbf{r}) \right\rangle = \sum_{\alpha=1}^{N}\sum_{\beta=1}^{N} \Delta T_\alpha \Delta T_\beta \sum_{n=1}^{N_\alpha}\sum_{m=1}^{N_\beta} \left\langle h^{\alpha n} h^{\beta m} f\left(\frac{|\mathbf{r}-\mathbf{b}^{\alpha n}|}{a_\alpha}\right) f\left(\frac{|\mathbf{r}-\mathbf{b}^{\beta m}|}{a_\beta}\right)\right\rangle. \tag{30}$$

Since the statistics are assumed homogeneous within the volume V, without loss of generality we may set $\mathbf{r}=0$. Furthermore, since the random sign factors and position vectors are independent random variables, the ensemble mean may be applied separately to functions of these variables:

$$\sigma^2 = \left\langle \Delta T^2(0) \right\rangle = \sum_{\alpha=1}^{N}\sum_{\beta=1}^{N} \Delta T_\alpha \Delta T_\beta \sum_{n=1}^{N_\alpha}\sum_{m=1}^{N_\beta} \left\langle h^{\alpha n} h^{\beta m}\right\rangle \left\langle f\left(\frac{b^{\alpha n}}{a_\alpha}\right) f\left(\frac{b^{\beta m}}{a_\beta}\right)\right\rangle. \tag{31}$$

Now, applying Equation (2b), this reduces to

$$\sigma^2 = \sum_{\alpha=1}^{N} \Delta T_\alpha^2 \sum_{n=1}^{N_\alpha} \left\langle f^2\left(\frac{b^{\alpha n}}{a_\alpha}\right)\right\rangle. \tag{32}$$

Since the positions of the QWs are uniformly distributed over the volume V, the ensemble mean of $f^2(b^{\alpha n}/a_\alpha)$ can be calculated by integrating the function over the volume and then dividing by V. The result is the same for each QW in a particular size class α. Furthermore, assuming that even the largest QWs are small compared to the size of the volume V, we may change variables to $\xi = b^{\alpha n}/a_\alpha$ and extend the limits of the integration to infinity. That is,

$$\left\langle f^2(b^{\alpha n}/a_\alpha)\right\rangle = V^{-1}\int_V d^3b f^2(b/a_\alpha) = (a_\alpha^3/V)\int d^3\xi f^2(\xi), \tag{33}$$

where the three-dimensional integral over ξ extends to infinity. Using this in Equation (32) yields

$$\sigma^2 = \sum_{\alpha=1}^{N} n_\alpha a_\alpha^3 \Delta T_\alpha^2 \int d^3\xi\, f^2(\xi) = (2\pi)^3 \sum_{\alpha=1}^{N} n_\alpha a_\alpha^3 \Delta T_\alpha^2 \int d^3 y F^2(y). \quad (34)$$

The second equality follows from Parseval's Theorem, $\int d^3\xi\, f^2(\xi) = (2\pi)^3 \int d^3 y F^2(y)$. This result is the same as Equation (6), after integrating both sides of that equation over the 3D wavenumber space. Hence we have shown that this alternative procedure for calculating the variance is consistent with previous results in the text.

We can perform the summation in Equation (34) by applying the scaling relationships, Equations (7). The result is

$$\sum_{\alpha=1}^{N} n_\alpha a_\alpha^3 \Delta T_\alpha^r = \phi \Delta T_1^r \sum_{\alpha=1}^{N} e^{-r\mu(\alpha-1)/3} = \phi \Delta T_1^r \frac{1 - e^{-r\mu N/3}}{1 - e^{-r\mu/3}}, \quad (35)$$

where the last term follows from the sum of the geometric series in the second term. If $\mu N \gg 1$, the exponential term in the numerator may be neglected. Furthermore, if the spacing between the size classes is small ($\mu \ll 1$), we may approximate $1 - e^{-r\mu/3} \simeq r\mu/3$. Under these conditions, which are typical, Equations (34) and (35) yield

$$\sigma^2 \approx \frac{3\phi}{2\mu} \Delta T_1^2 \int d^3\xi\, f^2(\xi). \quad (36)$$

For Gaussian QWs, $f(\xi) = (2\pi)^{3/2} \exp\left(-\xi^2/2\right)$, from which follows $\int d^3\xi\, f^2(\xi) = \pi^{3/2} (2\pi)^3$. We thus have $\sigma^2 \approx (3\phi/2\mu)\, \pi^{3/2} (2\pi)^3\, \Delta T_1^2$, in agreement with Equation (20).

Now let us turn to calculation of the fourth moment, which follows the same basic procedure as that for the second moment. Substituting Equation (1) into Equation (3), taking the fourth power and then the ensemble mean, and setting $\mathbf{r} = 0$, we have

$$\left\langle \Delta T^4 \right\rangle = \sum_{\alpha=1}^{N} \sum_{\beta=1}^{N} \sum_{\chi=1}^{N} \sum_{\gamma=1}^{N} \Delta T_\alpha \Delta T_\beta \Delta T_\chi \Delta T_\gamma\, S_{\alpha\beta\chi\gamma}, \quad (37a)$$

where

$$S_{\alpha\beta\chi\gamma} = \sum_{n=1}^{N_\alpha} \sum_{m=1}^{N_\beta} \sum_{p=1}^{N_\chi} \sum_{q=1}^{N_\gamma} \left\langle h^{\alpha n} h^{\beta m} h^{\chi p} h^{\gamma q} \right\rangle \left\langle f(\xi^{\alpha n}) f(\xi^{\beta m}) f(\xi^{\chi p}) f(\xi^{\gamma q}) \right\rangle, \quad (37b)$$

and

$$\xi^{\alpha n} = b^{\alpha n}/a_\alpha. \tag{37c}$$

Since the signs of the QWs are independent and have zero mean, the quantity $\langle h^{\alpha n} h^{\beta m} h^{\chi p} h^{\gamma q} \rangle$ is zero if any individual QW is represented just once [that is, if $(\alpha, n), (\beta, m), (\chi, p)$, or (γ, q) is unique]. The quantity $\langle h^{\alpha n} h^{\beta m} h^{\chi p} h^{\gamma q} \rangle$ is non-zero, equal to unity, when two distinct QWs are each represented twice $\big[(\alpha, n) = (\beta, m)$ and $(\chi, p) = (\gamma, q)$, but $(\alpha, n) \neq (\chi, p)$; $(\alpha, n) = (\chi, p)$ and $(\beta, m) = (\gamma, q)$, but $(\alpha, n) \neq (\beta, m)$; $(\alpha, n) = (\gamma, q)$ and $(\beta, m) = (\chi, p)$, but $(\alpha, n) \neq (\beta, m)\big]$, or when one distinct QW is represented four times $[(\alpha, n) = (\beta, m) = (\chi, p) = (\gamma, q)]$. We thus have

$$\begin{aligned}\langle h^{\alpha n} h^{\beta m} h^{\chi p} h^{\gamma q} \rangle = \delta_{\alpha\beta\chi\gamma}\delta_{nmpq} + \big(&\delta_{\alpha\beta}\delta_{nm}\delta_{\chi\gamma}\delta_{pq} + \delta_{\alpha\chi}\delta_{np}\delta_{\beta\gamma}\delta_{mq} \\ &+ \delta_{\alpha\gamma}\delta_{nq}\delta_{\beta\chi}\delta_{mp}\big)\big(1 - \delta_{\alpha\beta\chi\gamma}\delta_{nmpq}\big),\end{aligned} \tag{38}$$

where $\delta_{nmpq} = 1$ if and only if $n = m = p = q$. (Note that summation over repeated indices is not implicit here.) Substituting into the earlier result, and keeping in mind that all three groupings representing two QWs repeated twice must be equal, we have

$$\begin{aligned}\langle \Delta T^4 \rangle = &\sum_{\alpha=1}^{N} \Delta T_\alpha^4 \sum_{n=1}^{N_\alpha} \langle f^4(\xi^{\alpha n}) \rangle \\ &+ 3 \sum_{\alpha=1}^{N} \sum_{\beta=1}^{N} \Delta T_\alpha^2 \Delta T_\beta^2 \sum_{n=1}^{N_\alpha} \sum_{m=1}^{N_\beta} \big(1 - \delta_{\alpha\beta}\delta_{nm}\big) \langle f^2(\xi^{\alpha n}) f^2(\xi^{\beta m}) \rangle,\end{aligned} \tag{39}$$

where we used $\delta_{nmnm} = \delta_{nm}$. Furthermore, we may set

$$\langle f^2(\xi^{\alpha n}) f^2(\xi^{\beta m}) \rangle = \langle f^2(\xi^{\alpha n}) \rangle \langle f^2(\xi^{\beta m}) \rangle \tag{40}$$

in the quadruple summation, since the QWs are mutually independent and the term $(\alpha, n) = (\beta, m)$ is zero because of the presence of the $\big(1 - \delta_{\alpha\beta}\delta_{nm}\big)$ factor. Removing the term involving the Kronecker deltas from the quadruple summation, evaluating, and combining with the initial double summation, one has

$$\begin{aligned}\langle \Delta T^4 \rangle = &\sum_{\alpha=1}^{N} \Delta T_\alpha^4 \sum_{n=1}^{N_\alpha} \Big[\langle f^4(\xi^{\alpha n}) \rangle - 3 \langle f^2(\xi^{\alpha n}) \rangle^2\Big] \\ &+ 3 \sum_{\alpha=1}^{N} \sum_{\beta=1}^{N} \Delta T_\alpha^2 \Delta T_\beta^2 \sum_{n=1}^{N_\alpha} \sum_{m=1}^{N_\beta} \langle f^2(\xi^{\alpha n}) \rangle \langle f^2(\xi^{\beta m}) \rangle.\end{aligned}$$

Evaluating the ensemble averages and the sums over n and m by the same procedure applied to the calculation of the variance (see Equation (33)) yields

$$\langle \Delta T^4 \rangle = \sum_{\alpha=1}^{N} n_\alpha a_\alpha^3 \Delta T_\alpha^4 \int d^3\xi \; f^4(\xi) - 3 \sum_{\alpha=1}^{N} \frac{n_\alpha a_\alpha^6}{V} \Delta T_\alpha^4 \left[\int d^3\xi \; f^2(\xi) \right]^2 + 3 \left[\sum_{\alpha=1}^{N} n_\alpha a_\alpha^3 \Delta T_\alpha^2 \int d^3\xi \; f^2(\xi) \right]^2 .$$

The final summation within the square brackets is simply the variance. The middle summation should be much smaller than the first or third, since the volume V is chosen large enough that $a_\alpha^3 \ll V$ for all α. Hence we have for the kurtosis

$$\frac{\langle \Delta T^4 \rangle}{\sigma^4} \simeq 3 + \frac{1}{\sigma^4} \sum_{\alpha=1}^{N} n_\alpha a_\alpha^3 \Delta T_\alpha^4 \int d^3\xi \; f^4(\xi). \tag{41}$$

Using Equation (35) to calculate the sum, we have

$$\frac{\langle \Delta T^4 \rangle}{\sigma^4} = 3 + \frac{1}{\phi} \left[\frac{1 - e^{-4\mu N/3}}{1 - e^{-4\mu/3}} \int d^3\xi \, f^4(\xi) \right] \left[\frac{1 - e^{-2\mu N/3}}{1 - e^{-2\mu/3}} \int d^3\xi \, f^2(\xi) \right]^{-2}. \tag{42}$$

Applying the approximations $\mu N \gg 1$ and $\mu \ll 1$, this becomes

$$\frac{\langle \Delta T^4 \rangle}{\sigma^4} \approx 3 + \frac{\mu}{3\phi} \left[\int d^3\xi \, f^4(\xi) \right] \left[\int d^3\xi \, f^2(\xi) \right]^{-2}. \tag{43}$$

When the ratio ϕ/μ is large, the QWs are densely packed and the kurtosis is close to the value of 3 that is achieved with Gaussian statistics. When this ratio is small, the QWs are sparse and the kurtosis exceeds 3.

For a Gaussian QW, $\int d^3\xi \, f^4(\xi) = (\pi/2)^{3/2} (2\pi)^6$. Hence

$$\frac{\langle \Delta T^4 \rangle}{\sigma^4} = 3 + \frac{1}{(2\pi)^{3/2} \phi} \left[\frac{1 - e^{-4\mu N/3}}{1 - e^{-4\mu/3}} \right] \left[\frac{1 - e^{-2\mu N/3}}{1 - e^{-2\mu/3}} \right]^{-2} \approx 3 + \frac{\mu}{3 (2\pi)^{3/2} \phi}, \tag{44}$$

where again the approximation is valid for $\mu N \gg 1$ and $\mu \ll 1$.

Figure 6 plots the kurtosis vs. the packing fraction ϕ, as given by the exact form of Equation (44), for three sample choices of μ, namely, $\mu = 0.6931$, 0.1733, and 0.0433, which according to Equation (7) correspond to $a_\alpha / a_{\alpha+1} = 2, 2^{1/4}$, and $2^{1/16}$, respectively. In each case, N, the number of size classes, was chosen such that $a_1 / a_N = 2^{10} = 1024$, so $N = 1 + 10 \ln 2 / \mu$,

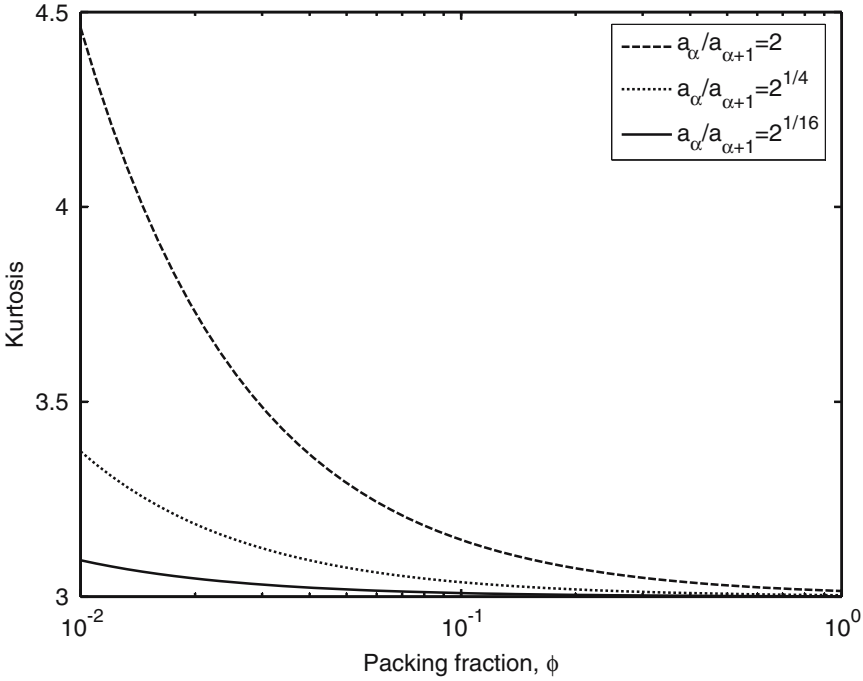

Figure 6. QW model kurtosis vs. packing fraction for three different size distributions.

or $N = 11$, 41, and 161, respectively. Note that $\mu N = 7.931$ in all cases, large enough to neglect the exponentials in the numerators of each factor in Equation (44). We see that when there is a large spacing between the size classes, e.g. $a_\alpha/a_{\alpha+1} = 2$, the packing fraction must be close to unity to obtain a kurtosis near 3. A nearly continuous range of sizes, e.g. $a_\alpha/a_{\alpha+1} = 2^{1/16}$, allows this for a much smaller packing fraction.

2.6. Example visualizations

In this subsection, we present visualizations of several turbulent temperature fluctuation fields that have been synthesized by the QW method. Figures 7–9 are grey-scale plots of fields obtained with Gaussian QWs, for three different choices of the parameter set $[\mu, \phi, N]$, as indicated in the figure captions. The QWs were randomly positioned inside a rectangular volume V having dimensions 150 m by 150 m by 50 m. The visualizations show a 100 m by 100 m cross-section in the x–y plane through the volume V, at $z = 25$ m. (A 25-m buffer on each side of this cross-section mitigates edge effects that otherwise would result from missing large QWs that are partly inside V but whose centres lie outside of V.) In each case, the largest QW size is $a_1 = 50$ m. QWs with size less than 0.5 m are not generated, since they would not be visible at the resolution of the visualizations.

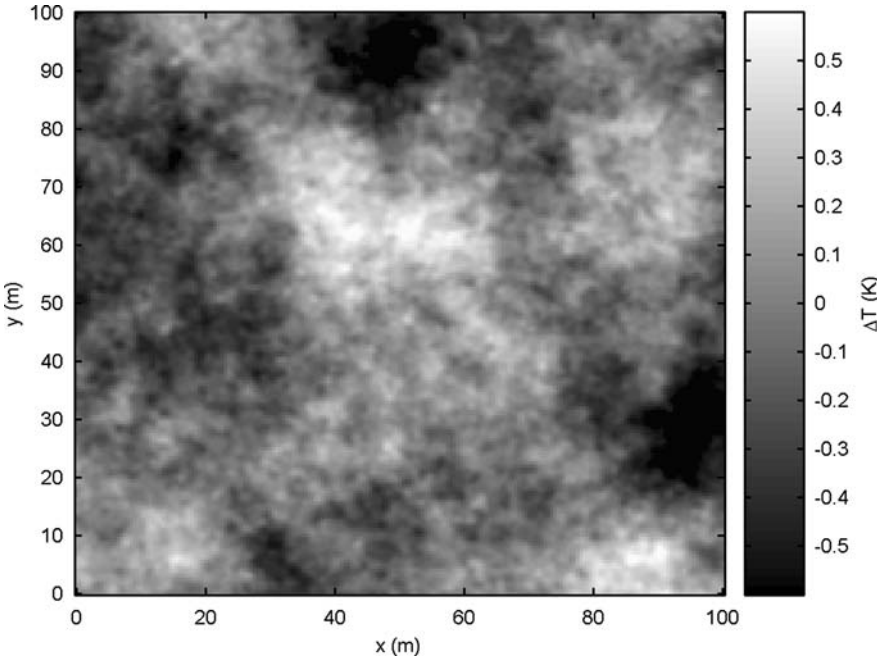

Figure 7. Visualization of a QW simulation of turbulent temperature fluctuations in two dimensions, with parameters $\mu = 0.693$, $\phi = 1$, kurtosis = 3.01, and $N = 7$.

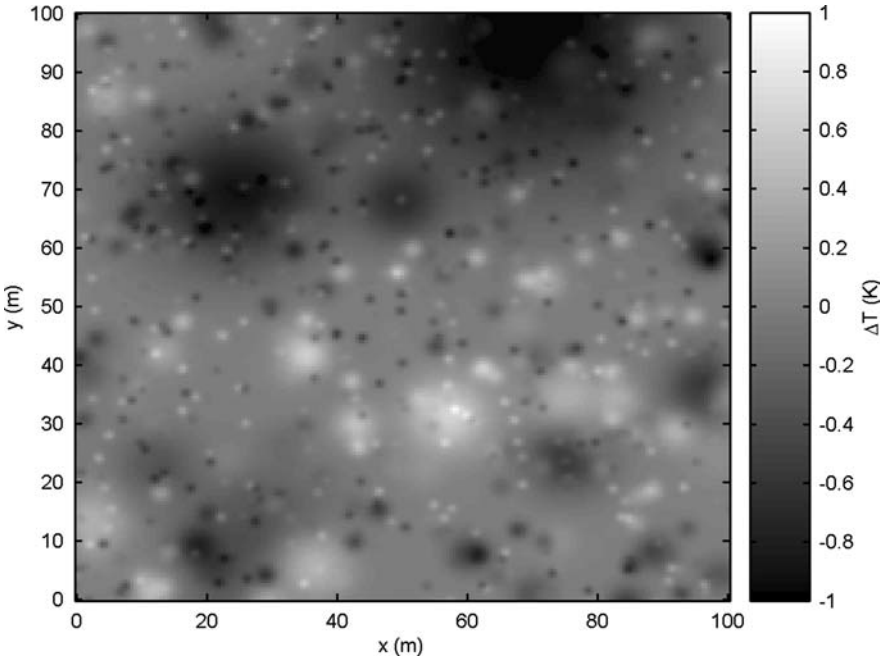

Figure 8. Visualization of a QW simulation of turbulent temperature fluctuations in two dimensions, with parameters $\mu = 0.693$, $\phi = 0.01$, kurtosis = 4.47, and $N = 7$.

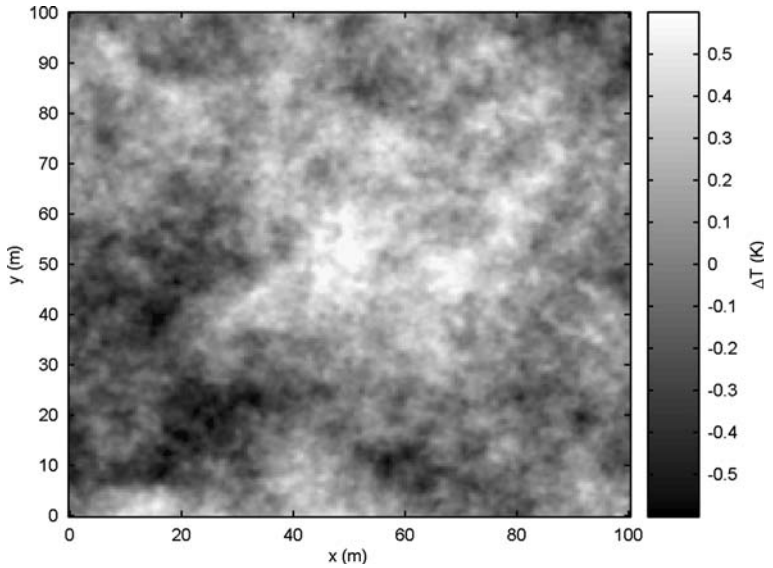

Figure 9. Visualization of a QW simulation of turbulent temperature fluctuations in two dimensions, with parameters $\mu = 0.0433$, $\phi = 0.0625$, kurtosis = 3.01, and $N = 107$.

The constant C_1 [see Equations (9–11)] was chosen to be $8.82 \times 10^5\,\mathrm{m^3\,K^2}$, which corresponds to a QW temperature amplitude $\Delta T_1 = 0.14\,\mathrm{K}$ in Figures 7 and 9, and $\Delta T_1 = 1.4\,\mathrm{K}$ in Figure 8. The plots are obtained by subdividing the visualization plane into a fine mesh of squares of area $\Delta A = 0.5\,\mathrm{m}$ by 0.5 m, and then, after all the QWs have been chosen and positioned, evaluating the double sum in Equation (3) at the centre point of each square.

One noteworthy feature of these QW simulations is the realistic appearance of the simulated fields exhibited by Figures 7 and 9. Note that Figure 7 results from a large packing fraction, $\phi = 1$, and a quite discontinuous set of sizes, $a_\alpha / a_{\alpha+1} = 2 (\mu = 0.693)$, while Figure 9 results from a small packing fraction, $\phi = 0.0625$, and a nearly continuous set of sizes, $a_\alpha / a_{\alpha+1} = 2^{1/16} (\mu = 0.0433)$. However, these two cases were chosen to have the same value of the kurtosis, 3.01.

Another noteworthy feature is exhibited by Figure 8, namely, the unrealistic appearance of the simulated turbulent field in this case. Since Figure 8 results from a small packing fraction, $\phi = 0.01$, as well as the same discontinuous set of sizes used for Figure 7, $a_\alpha / a_{\alpha+1} = 2 (\mu = 0.693)$, this appearance is not surprising. Note that this case has a kurtosis value of 4.47.

3. Discussion

In this paper, we used a very simple QW model of turbulent temperature fluctuations: it employs spherically symmetric spectral parent functions that

are positive-valued at $k = 0$, uniformly random locations of the QWs in the volume containing the turbulence, and no correlations among the signs of the temperature fluctuations of different QWs. The model also uses the scaling relations of Equation (7), which are not unique. They were chosen by Goedecke and Auvermann (1997) as perhaps the simplest ones that agree with the Kolmogorov energy transfer model of fully developed turbulence and also yield the correct Kolmogorov behaviour of temperature and velocity spectra in the inertial subrange. Alternatives were discussed briefly in that paper, but they have not yet been pursued.

In Section 2, we accomplished the main goals stated in the Introduction. First, in Section 2.3 we showed that this simplest QW model can reproduce any given spectrum of isotropic homogeneous temperature fluctuations quite accurately. In particular, the matching condition of Equation (12) determines a QW spectral parent function that would reproduce such a given spectrum exactly, at all wavenumbers, if it were inserted into Equation (9). However, Equation (12) appears difficult to solve. We noted that, for typical ratios of the smallest to the largest QW sizes, the second term on the right-hand side of Equation (12) is negligible for wavenumbers smaller than those in the dissipation range. Since the given spectral behaviour in that range is generally neither accurate nor important to our applications, we dropped that second term. The resulting Equation (13) then yields a spectral parent function that reproduces almost any given isotropic spectrum virtually exactly in the energy, transition, and inertial subranges. We treated the von Kármán spectrum as an example of a given spectrum, and solved Equation (13) for the von Kármán spectral parent function (Equation (15)). We also obtained an integral expression for the corresponding spatial parent function (Equation (16)).

Second, in Section 2.4 we showed that, if we use any localized QW parent function (other than the one given by Equations (12) or (13)) in this simplest QW model, the resulting spectrum could be matched exactly to a given isotropic spectrum in both the inertial and the energy subranges, but matched only approximately in the energy-to-inertial transition subrange. Actually, we showed this only by example, using a Gaussian QW parent function and the von Kármán spectrum as the given one, but the generalization is obvious by observation of Equation (9). In the example, the mismatch in the transition subrange led to substantial disagreement between the variances of the two fluctuations. We also showed that, if we required the Gaussian QW fluctuations to have the same variance as the von Kármán fluctuations, then the spectra would differ noticeably everywhere except in the inertial subrange, where of course we required them to be the same.

Third, in Section 2.5 we derived analytic expressions for the kurtosis of a QW representation in terms of the QW model parameters ϕ, the packing

fraction, and μ, the natural logarithm of the ratio of adjacent QW sizes (see Equations (7)). We showed that the kurtosis differs appreciably from the value 3 only if the ratio ϕ/μ is small.

Fourth, in Section 2.6 we provided grey-scale visualizations of several two-dimensional QW model simulations, for different choices of ϕ and μ. These visualizations revealed that a large kurtosis does not seem to produce a realistic appearance of the model turbulent field, while a kurtosis near the limiting value of 3 does. This possible connection between values of the kurtosis and the visual appearance of the simulated turbulent fields needs to be investigated in further study.

Generalizations of the simple QW model used herein would be necessary if measured spectra do not have the isotropic translation-invariant behaviour assumed above. For example, anisotropic inhomogeneous fluctuations could not be represented by spherically symmetric QWs, nor could the QWs be uniformly distributed in space. QW representations of inhomogeneity and intermittency would require changes in the model, such as spatially dependent parameters and scale-dependent packing fractions. For another example, suppose a measured isotropic spectrum is not constant in the energy subrange. Then its QW model might have to include more complicated parent functions, or correlations among the signs of the QWs, or volume scale effects, or some other changes that could accommodate the observed energy subrange behaviour. These kinds of modifications remain to be investigated in future work.

Acknowledgements

This material is partly based on work supported by the U.S. Army Research Office under contracts DAAG19-01-1-0640 and DAAD19-03-1-0104.

References

Boulanger, P., Raspet, R., and Bass, H. E.: 1995, 'Sonic Boom Propagation through a Realistic Turbulent Atmosphere', *J. Acoust. Soc. Amer*. **98**, 3412–3417.

De Wolf, D. A.: 1993, 'A Random Motion Model of Fluctuations in a Nearly Transparent Medium', *Radio Sci.* **18**, 138–142.

Fung, J. C. H., Hunt, J. C. R., Malik, N. A., and Perkins, R. J.: 1992, 'Kinematic Simulation of Homogeneous Turbulence by Unsteady Random Fourier Modes', *J. Fluid Mech.* **236**, 231–318.

Goedecke, G. H. and Auvermann, H. J.: 1997, 'Acoustic Scattering by Atmospheric Turbules', *J. Acoust. Soc. Amer.* **102**, 759–771.

Goedecke, G. H., Wood, R. C., Auvermann, H. J., Ostashev, V. E., Havelock, D. I., and Ting, C.: 2001a, 'Spectral Broadening of Sound Scattered by Advecting Atmospheric Turbulence', *J. Acoust. Soc. Amer.* **109**, 1923–1934.

Goedecke, G. H., Moore, S. M., Auvermann, H. J., and Ostashev, V. E.: 2001b, 'Quasi-wavelet Model of Anisotropic Inhomogeneous Turbulence', *Proceedings, Battlespace Atmospheric and Cloud Impacts on Military Operations Conference* (BACIMO 2001), ARL-SR-01126, July 10–12, 2001. Available on CD-ROM from the Cooperative Institute for Research in the Atmosphere, Colorado State University, Fort Collins, CO, 80523.

Goedecke, G. H., Ostashev, V. E., and Wilson, D. K.: 2004a, 'Quasi-wavelet Models of Turbulent Temperature and Shear-driven Velocity Fluctuations', *Proceedings, 11th Long Range Sound Propagation Symposium,* Lake Morey, VT, June, 2004. Available on CD-ROM from the National Center for Physical Acoustics, University of Mississippi, Coliseum Drive, University, MS, 38677.

Goedecke, G. H., Ostashev, V. E., Wilson, D. K., and Auvermann, H. J.: 2004b, 'Quasi-wavelet Model of von Kármán Spectrum of Turbulent Velocity Fluctuations', *Boundary-Layer Meteorol.* **112**, 33–56.

Gradshteyn, I. S. and Rhyzik, I. M.: 1980, *Table of Integrals, Series, and Products,* corrected and enlarged edition prepared by Alan Jeffrey, Academic Press, New York, 1160 pp.

Mann, J.: 1994, 'The Spatial Structure of Neutral Atmospheric Surface Layer Turbulence', *J. Fluid Mech.* **273**, 141–168.

Marlin, D. H., Aldridge, D. F., Symons, N. P., Wilson, D. K., and Ostashev, V. E.: 2003, 'Finite-difference Time-Domain Acoustic Wave Propagation in Complex Atmospheric Environments: Second Year Results', *Proceedings, Military Sensing Symposium on Battlefield Acoustic and Seismic Sensing*. Laurel, MD, October 7–10, 2003. Published by Infrared Information Analysis Center, P. O. Box 134008, Ann Arbor, MI, 48113.

McBride, W. E., Bass, H. E., Raspet, R., and Gilbert, K. E.: 1992, 'Scattering of Sound by Atmospheric Turbulence: Predictions in a Refractive Shadow Zone', *J. Acoust. Soc. Amer*. **91**, 1336–1340.

Nelkin, M.: 1992, 'In What Sense is Turbulence an Unsolved Problem', *Science* **255**, 566–570.

Van Renterghem, T.: 2003, *The Finite-difference Time-Domain Method for Simulation of Sound Propagation in a Moving Medium,* Doctoral Thesis, Universiteit Gent.

Vecherin, S. N., Ostashev, V. E., Wilson, D. K., Voronovich, A. G., Goedecke, G. H., Collier, S. L., Noble, J. M., and Ligon, D.: 2004, 'Forward and Inverse Problems of Acoustic Tomography of the Atmosphere', *Proceedings, 11th Long Range Sound Propagation Symposium,* Lake Morey, VT, June 2004. Available on CD-ROM from the National Center for Physical Acoustics, University of Mississippi, Coliseum Drive, University, MS, 38677.

Wilson, D. K., Moran, M. L., Liu, L., Ostashev, V. E., Aldridge, D. F., Symons, N. P., and Marlin, D. H.: 2003, 'Development of a High-Fidelity Simulation Capability for Battlefield Acoustics', *Proceedings, SPIE AeroSense 2003*, Orlando, FL., 2003. Available on-line from http://spie.org/.

Wilson, D. K., Ostashev, V. E., Goedecke, G. H., and Auvermann, H. J.: 2004a, 'Quasi-wavelet Calculations of Sound Scattering Behind Barriers', *Appl. Acoust.* **65**, 605–627.

Wilson, D. K., Ostashev, V. E., Vecherin, S. N., Voronovich, A. G., Collier, S. L., and Noble, J. M.: 2004b, 'Assessment of Acoustic Travel-Time Tomography of the Atmospheric Surface Layer', *Proceedings, 16th Symposium on Boundary Layers and Turbulence*, Portland, ME., August 9–13, 2004. American Meteorological Society, Boston, MA, CD-ROM paper 6.9.